REPORT_RAPPORT_

MAS

Modelling, Analysis and Simulation

Modelling, Analysis and Simulation

Statistical mechanics of Arakawa's discretizations

S.B. Dubinkina, J.E. Frank

Centrum voor Wiskunde en Informatica (CWI) is the national research institute for Mathematics and Computer Science. It is sponsored by the Netherlands Organisation for Scientific Research (NWO).
CWI is a founding member of ERCIM, the European Research Consortium for Informatics and Mathematics.

CWI's research has a theme-oriented structure and is grouped into four clusters. Listed below are the names of the clusters and in parentheses their acronyms.

Probability, Networks and Algorithms (PNA)

Software Engineering (SEN)

Modelling, Analysis and Simulation (MAS)

Information Systems (INS)

Statistical mechanics of Arakawa's discretizations

ABSTRACT

The results of statistical analysis of simulation data obtained from long-time integrations of geophysical fluid models greatly depend on the conservation properties of the numerical discretization chosen. Statistical mechanical theories are constructed for three discretizations of the quasi-geostrophic model due to Arakawa (1966), each having different conservation properties. It is shown that the three statistical theories accurately explain the differences observed in statistics derived from the discretizations. The effect of the time discretization is also considered, and it is shown that projection is insufficient if the underlying spatial discretization is not conservative.

Statistical mechanics of Arakawa's discretizations

Svetlana Dubinkina, Jason Frank

CWI

P.O. Box 94079, 1090 GB Amsterdam, The Netherlands

ABSTRACT

The results of statistical analysis of simulation data obtained from long-time integrations of geophysical fluid models greatly depend on the conservation properties of the numerical discretization chosen. Statistical mechanical theories are constructed for three discretizations of the quasi-geostrophic model due to Arakawa (1966), each having different conservation properties. It is shown that the three statistical theories accurately explain the differences observed in statistics derived from the discretizations. The effect of the time discretization is also considered, and it is shown that projection is insufficient if the underlying spatial discretization is not conservative.

1. INTRODUCTION

In applications such as weather and climate predictions, long numerical simulations are carried out for dynamical systems that are known to be chaotic, and as a result, for which it is impossible to simulate a particular solution with any accuracy in the usual sense of numerical analysis. Instead, the goal of such simulations is to obtain a data set suitable for computing statistical averages or otherwise to sample the probability distribution associated with the continuous problem.

However it known that different discretizations have very different properties—backward error analysis ([23, 24, 6, 9]) stresses viewing the discrete solution as being sampled from a perturbed problem—and the effects of these different properties become more pronounced when the numerical map is iterated over a very large number of time steps. Therefore it is important to establish the influence the method has on the statistical results. Preferably, one would like to determine creteria a method should satisfy to yield meaningful statistics, and to understand statistical accuracy in terms of discretization parameters.

In this paper, we adapt the statistical mechanics theory of 2D ideal fluids—as first developed by Kraichnan [8] and Salmon et al. [21], and recently expounded in Majda & Wang [11]—to the semi-discretizations proposed by Arakawa [2] for an ideal fluid in vorticity-stream function form. Arakawa's discretizations conserve energy (E), enstrophy (Z), or both (EZ), and we construct a statistical mechanics theory for each discretization. The resulting theories give entirely different predictions for the statistical behavior of the methods. Numerical experiments with conservative and projected time integrators agree with the statistical predictions, confirming that the conservation properties of a method define the backdrop, or climatic mean, against which the dynamics takes place. A further experiment, using a non-conservative spatial discretization, coupled with projection onto the energy and/or enstrophy manifolds, yields statistics that disagree with the theories, suggesting that local conservation is crucial.

It should be mentioned at the outset that the statistical theory is a model and is known to be incomplete. In [1], Abramov & Majda show that nonzero values of the third moment of potential vorticity can cause significant deviation from the statistical predictions. On the other hand, the third moment cannot be incorporated into the equilibrium statistical mechanics distribution, because it is non-normalizable. In Section 6 we use the numerical setup of [1] to facilitate comparison with their results. We wish to stress, however, that the focus of this article is not the statistical mechanics of ideal fluids *per se*, but rahter the application of statistical mechanics as a tool for the numerical analysis of discretizations.

In Section 2 we recall the quasi-geostrophic potential vorticity equation and its conservation properties. Section 3 reviews Arakawa's discretizations. In Section 4, the equilibrium statistical mechanical theories are developed for the three discretizations. Time integration aspects are discussed in Section 5. The numerical experiments confirming the statistical predictions are presented in Section 6.

2. The quasi-geostrophic model

This paper addresses the statistical behavior of conservative discretizations of the quasi-geostrophic potential vorticity model (QG) on a doubly periodic domain, $\Omega = \{\boldsymbol{x} = (x, y) \,|\, x, y \in [0, 2\pi]\}$. The QG equation [17, 18] is

$$q_t = \mathcal{J}(q, \psi), \tag{2.1a}$$
$$\Delta \psi = q - h, \tag{2.1b}$$

where the potential vorticity (PV) $q(\boldsymbol{x}, t)$, the stream function $\psi(\boldsymbol{x}, t)$, and the orography $h(\boldsymbol{x})$ are scalar fields, periodic in x and y with period 2π. The Laplacian operator is denoted by Δ, and the operator $\mathcal{J}$ is defined by

$$\mathcal{J}(q, \psi) := q_x \psi_y - q_y \psi_x. \tag{2.2}$$

The QG equation is a Hamiltonian PDE [14] having Poisson bracket

$$\{\mathcal{F}, \mathcal{G}\} = \int q \mathcal{J}\left(\frac{\delta \mathcal{F}}{\delta q}, \frac{\delta \mathcal{G}}{\delta q}\right) d\boldsymbol{x} \tag{2.3}$$

and Hamiltonian functional

$$\mathcal{E}[q] = -\frac{1}{2} \int \psi \cdot (q - h) \, d\boldsymbol{x}. \tag{2.4}$$

The Poisson bracket is degenerate with Casimir invariants the generalized enstrophies $\mathcal{C}[q] = \int f(q) \, d\boldsymbol{x}$ for arbitrary function f. In particular, the polynomial enstrophies

$$\mathcal{C}_p[q] = \int q^p \, d\boldsymbol{x}, \qquad p = 1, 2, \dots$$

are conserved, of which the most important—the second moment of vorticity $\mathcal{C}_2$—will be denoted by $\mathcal{Z}$

$$\mathcal{Z}[q] = \frac{1}{2} \int q^2 \, d\boldsymbol{x}, \tag{2.5}$$

and will henceforth be referred to as *the* enstrophy.

3. Spatial semi-discretization

We first consider the discretization of (2.1) in space only. The resulting system of ordinary differential equations will be referred to as the semi-discretization, and we will primarily be concerned with its analysis and statistical mechanics.

When discretizing Hamiltonian PDEs, it is advisable to consider the discretizations of the Poisson bracket and the Hamiltonian separately. As noted in [12], if a discrete Poisson bracket can be constructed to maintain skew-symmetry and satisfy the Jacobi identity, then any quadrature for the Hamiltonian will yield a semi-discretization that is a Hamiltonian ODE, and as a result will conserve energy and (possibly some subclass of) Casimirs. Similarly, from the point of view of statistical mechanics, it is also useful to consider the discretizations of the bracket and the Hamiltonian separately. The bracket ensures the conservation of energy and enstrophy and preservation of volume, which are necessary ingredients for the *existence* of a statistical theory at all. But only the conserved quantities themselves enter into the probability distribution. Thus the *predictions* of the theory depend only on the discretization of these conserved quantities. The discretization of the Hamiltonian (2.4) amounts to a choice for the discrete Laplacian in (2.1b) and will be treated in Section 3.1. The bracket will be discretized with Arakawa's schemes in section 3.2.

For Eulerian fluid models, the only known discretization with Poisson structure is the sine-bracket truncation of Zeitlin [25], which is limited to 2D, incompressible flows on periodic geometry. This truncation has spectral accuracy and conserves M polynomial enstrophies on an $M \times M$ grid. Its statistics are investigated in [1]. For more general fluid problems, no Poisson discretizations are available. In lieu of a semi-discretization with Poisson structure, one may attempt to construct discretizations which conserve desired first integrals and are volume preserving. The flow of energy is important for statistics, and the spatial discretization determines the local flow. In numerical weather prediction, energy conserving discretizations were advocated by Lorenz in 1960 [10]. Motivated by Lorenz's work, Arakawa [2] constructed discretizations that conserved energy, enstrophy or both. As we will see, these discretizations are also all volume preserving.

We discretize (2.1) on a uniform $M \times M$ grid. Let $\Delta x = \Delta y = 2\pi/M$ and consider a grid function $\boldsymbol{q}(t) \in \mathrm{R}^{M \times M}$, where $q_{\boldsymbol{m}}(t) = q_{m_1,m_2}(t) \approx q(m_1 \Delta x, m_2 \Delta y, t)$, $m_1, m_2 = 0, \ldots, M-1$, with periodicity realized by identifying the indices M and 0. We think of $\boldsymbol{q}$ as a vector in an M^2-dimensional phase space; that is, we identify R^{M^2} and $\mathrm{R}^{M \times M}$, and use vector notation, e.g., $\boldsymbol{q}^T \boldsymbol{q}$ for the vector inner product of such a vector with itself.

3.1 Spectral solution of the stream function

The linear elliptic PDE (2.1b) is solved using the Fourier spectral method. Let the Fourier transform of $\boldsymbol{q} \in \mathrm{R}^{M \times M}$ be defined by

$$\hat{\boldsymbol{q}} = \mathcal{F}\boldsymbol{q} \quad \Longleftrightarrow \quad \hat{q}_{\boldsymbol{k}} = \frac{1}{M} \sum_{m_1,m_2=0}^{M-1} q_{\boldsymbol{m}} e^{-i(\boldsymbol{m}\cdot\boldsymbol{k})}, \quad k_1, k_2 = -M/2+1, \ldots, M/2. \qquad (3.1)$$

The inverse transform is $\mathcal{F}^{-1} = \mathcal{F}^*$, and, for later reference, Parseval's identity reads

$$\sum_{m_1,m_2} q_{\boldsymbol{m}}^2 = \sum_{k_1,k_2} |\hat{q}_{\boldsymbol{k}}|^2.$$

Equation (2.1b) is solved exactly in Fourier-space. Denote the discrete Laplacian operator by Δ_M:

$$\Delta_M \boldsymbol{\psi} = \boldsymbol{q} - \boldsymbol{h} \iff -|\boldsymbol{k}|^2 \hat{\psi}_{\boldsymbol{k}} = \hat{q}_{\boldsymbol{k}} - \hat{h}_{\boldsymbol{k}}, \quad k_1, k_2 = -M/2+1, \ldots M/2, \qquad (3.2)$$

where $|\boldsymbol{k}|^2 = k_1^2 + k_2^2$. This relation is solved for stream function field $\boldsymbol{\psi}$ with mean zero. The inverse Laplacian restricted to the hyperplane $\hat{\psi}_{0,0} \equiv 0$ is denoted by Δ_M^{-1}, i.e.

$$\boldsymbol{\psi} = \Delta_M^{-1}(\boldsymbol{q} - \boldsymbol{h}) \quad \Longleftrightarrow \quad \hat{\psi}_{\boldsymbol{k}} = \begin{cases} -|\boldsymbol{k}|^{-2}(\hat{q}_{\boldsymbol{k}} - \hat{h}_{\boldsymbol{k}}), & \boldsymbol{k} \neq 0, \\ 0, & \boldsymbol{k} = 0. \end{cases}$$

3.2 Arakawa's discretizations

Arakawa [2] constructed finite difference discretizations of (2.2) that preserve discrete versions of energy (2.4), enstrophy (2.5), or both.

Define matrices D_x and D_y that implement the standard second order central difference approximations to the first derivative

$$(D_x \boldsymbol{q})_{m_1, m_2} = \frac{q_{m_1+1, m_2} - q_{m_1-1, m_2}}{2 \triangle x}, \qquad (D_y \boldsymbol{q})_{m_1, m_2} = \frac{q_{m_1, m_2+1} - q_{m_1, m_2-1}}{2 \triangle y}.$$

These matrices are skew-symmetric: $D_x^T = -D_x$, $D_y^T = -D_y$. Additionally, denote the element-wise product of two vectors by $(\boldsymbol{u} * \boldsymbol{v})_{\boldsymbol{m}} = u_{\boldsymbol{m}} v_{\boldsymbol{m}}$. The scalar product

$$\boldsymbol{u}^T (\boldsymbol{v} * \boldsymbol{w}) = \sum_k u_k v_k w_k \tag{3.3}$$

is fully symmetric with respect to the vectors $\boldsymbol{u}$, $\boldsymbol{v}$ and $\boldsymbol{w}$.

Arakawa's discretizations can be viewed as discrete approximations to the equivalent formulations of (2.2)

$$\mathcal{J}(q, \psi) = q_x \psi_y - q_y \psi_x,$$
$$\mathcal{J}(q, \psi) = \partial_x(q \psi_y) - \partial_y(q \psi_x),$$
$$\mathcal{J}(q, \psi) = \partial_y(q_x \psi) - \partial_x(q_y \psi),$$

and are given by

$$J_0(\boldsymbol{q}, \boldsymbol{\psi}) := (D_x \boldsymbol{q}) * (D_y \boldsymbol{\psi}) - (D_y \boldsymbol{q}) * (D_x \boldsymbol{\psi}), \tag{3.4}$$
$$J_E(\boldsymbol{q}, \boldsymbol{\psi}) := D_x(\boldsymbol{q} * D_y \boldsymbol{\psi}) - D_y(\boldsymbol{q} * D_x \boldsymbol{\psi}), \tag{3.5}$$
$$J_Z(\boldsymbol{q}, \boldsymbol{\psi}) := D_y(\boldsymbol{\psi} * D_x \boldsymbol{q}) - D_x(\boldsymbol{\psi} * D_y \boldsymbol{q}). \tag{3.6}$$

The Arakawa schemes are interesting for us, because they are all based on the standard second order central difference operators applied in various 'conservation forms' and hence, for short simulations with smooth solutions, there is often little noticeable difference between different discretizations. One might therefore expect that they yield similar statistics. On the contrary, the statistical behavior is dramatically different.

To understand the conservation properties of these three discretizations, it is useful to introduce the Nambu bracket formalism [15, 16, 20]. Define the associated brackets (the gradients are with respect to $\boldsymbol{q}$)

$$\begin{aligned}
\{F, G, H\}_0 &:= -\nabla F^T J_0(\nabla G, \nabla H) \\
&= -\nabla F^T \left[(D_x \nabla G) * (D_y \nabla H) - (D_y \nabla G) * (D_x \nabla H) \right], \\
\{F, G, H\}_E &:= -\nabla F^T J_E(\nabla G, \nabla H) \\
&= -\nabla F^T \left[D_x(\nabla G * D_y \nabla H) - D_y(\nabla G * D_x \nabla H) \right], \\
\{F, G, H\}_Z &:= -\nabla F^T J_E(\nabla G, \nabla H) \\
&= -\nabla F^T \left[D_y(D_x \nabla G * \nabla G) - D_x(D_y \nabla G * \nabla H) \right],
\end{aligned}$$

for arbitrary differentiable $F(\boldsymbol{q})$, $G(\boldsymbol{q})$, $H(\boldsymbol{q}) : \mathrm{R}^{M^2} \to \mathrm{R}$.

Then second order consistent discretizations of (2.1) are obtained in the bracket with E_M and Z_M according to:

$$\dot{q}_{\boldsymbol{m}} = \{q_{\boldsymbol{m}}, Z_M, E_M\},$$

where E_M and Z_M are discrete approximations to the energy

$$E_M(\boldsymbol{q}) = -\frac{1}{2}\boldsymbol{\psi}^T(\boldsymbol{q} - \boldsymbol{h})\Delta x \Delta y = \frac{1}{2}\sum_{\boldsymbol{k}}|\boldsymbol{k}|^2|\hat{\psi}_{\boldsymbol{k}}|^2 \Delta x \Delta y \tag{3.7}$$

and enstrophy

$$Z_M(\boldsymbol{q}) = \frac{1}{2}\boldsymbol{q}^T\boldsymbol{q}\Delta x \Delta y = \frac{1}{2}\sum_{\boldsymbol{k}}|\hat{q}_{\boldsymbol{k}}|^2 \Delta x \Delta y. \tag{3.8}$$

The Lie derivative $\frac{dF}{dt}$ of a function $F(\boldsymbol{q})$ along a solution to the discrete equations is given by the Nambu bracket of F with Z_M and E_M:

$$\frac{dF}{dt} = \{F, Z_M, E_M\}.$$

This fact can be used to establish the conservation properties of the various discretizations.

First note that the bracket $\{\cdot, \cdot, \cdot\}_0$ is antisymmetric in its last two arguments, due to the commutativity of the $*$ operator:

$$\{F, G, H\}_0 = -\{F, H, G\}_0. \tag{3.9}$$

Next, using the skew-symmetry of D_x and D_y and the symmetry of (3.3), we observe that

$$\{F, G, H\}_E = (D_x \nabla F)^T (\nabla G * D_y \nabla H) - (D_y \nabla F)^T (\nabla G * D_x \nabla H) = \{G, H, F\}_0,$$

and similarly,

$$\{F, G, H\}_Z = \{H, F, G\}_0.$$

It follows that the J_E discretization conserves energy, since

$$\frac{dE_M}{dt} = \{E_M, Z_M, E_M\}_E = \{Z_M, E_M, E_M\}_0 = 0$$

by the antisymmetry property (3.9). By the same token, J_Z conserves enstrophy:

$$\frac{dZ_M}{dt} = \{Z_M, Z_M, E_M\}_Z = \{E_M, Z_M, Z_M\}_0 = 0.$$

Furthermore, a fully antisymmetric Jacobian can be derived as an average of (3.4)–(3.6)

$$J_{EZ}(\boldsymbol{q}, \boldsymbol{\psi}) = \frac{1}{3}\left[J_0(\boldsymbol{q}, \boldsymbol{\psi}) + J_E(\boldsymbol{q}, \boldsymbol{\psi}) + J_Z(\boldsymbol{q}, \boldsymbol{\psi})\right], \tag{3.10}$$

and the associated bracket

$$\begin{aligned}\{F, G, H\}_{EZ} &:= \frac{1}{3}\left(\{F, G, H\}_0 + \{F, G, H\}_E + \{F, G, H\}_Z\right) \\ &= \frac{1}{3}\left(\{F, G, H\}_0 + \{G, H, F\}_0 + \{H, F, G\}_0\right)\end{aligned}$$

is fully antisymmetric (with respect to transposition of any two elements). For example, transposing G and H yields

$$\begin{aligned}\{F, H, G\}_{EZ} &= \frac{1}{3}\left(\{F, H, G\}_0 + \{H, G, F\}_0 + \{G, F, H\}_0\right) \\ &= \frac{1}{3}\left(-\{F, G, H\}_0 - \{H, F, G\}_0 - \{G, H, F\}_0\right) = -\{F, G, H\}_{EZ}.\end{aligned}$$

As a result, this bracket conserves *both* invariants (3.7) and (3.8).

One can check that a solution of the form $\boldsymbol{q} = \mu\boldsymbol{\psi}$ is an exact steady state for the discretizations J_0 and J_{EZ}. Such a solution is not, in general, a steady state solution for discretizations J_E and J_Z. However, the limit cases $\{\boldsymbol{\psi} \equiv 0, \boldsymbol{q} = \boldsymbol{h}\}$ and $\{\boldsymbol{q} \equiv 0, \boldsymbol{\psi} = -\Delta_M^{-1}\boldsymbol{h}\}$ obviously *are* steady states to those discretizations.

3.3 Volume preservation

In addition to conservation, a second important ingredient for statistical mechanics is the preservation, by the flow map, of the phase space volume element. In this section we demonstrate that each of the discretizations from the previous section is volume preserving. Let us define the matrix $D(\boldsymbol{a}) = \operatorname{diag}(\boldsymbol{a})$ to be the diagonal matrix whose diagonal elements are the components of the vector $\boldsymbol{a}$ (i.e. $D(\boldsymbol{a})_{ij} = a_i \delta_{ij}$).

Recall that for an ODE

$$\boldsymbol{y}' = \boldsymbol{f}(\boldsymbol{y})$$

the divergence of the vector field $\boldsymbol{f}$ satisfies

$$\operatorname{div} \boldsymbol{f} = \operatorname{tr}(\boldsymbol{f}'),$$

where $\boldsymbol{f}'$ denotes the Jacobian matrix of $\boldsymbol{f}$. In particular, for a matrix A, $\operatorname{div} A\boldsymbol{f}(\boldsymbol{y}) = \operatorname{tr}(A\boldsymbol{f}')$. Furthermore, for

$$\boldsymbol{y}' = \boldsymbol{f}(\boldsymbol{y}) = \boldsymbol{g}(\boldsymbol{y}) * \boldsymbol{h}(\boldsymbol{y})$$

it holds that

$$\boldsymbol{f}' = D(\boldsymbol{g})\boldsymbol{h}' + D(\boldsymbol{h})\boldsymbol{g}'.$$

In the following calculations we make ready use of the commutative and transpose properties of the trace $\operatorname{tr}(AB) = \operatorname{tr}(BA) = \operatorname{tr}(B^T A^T)$. We also need the following properties of our discretization matrices. The difference operators D_x and D_y are skew-symmetric and commute $D_x D_y - D_y D_x = 0$. The discrete inverse Laplacian matrix Δ_M^{-1} is symmetric and represents a central finite difference stencil. In this case, the matrices $D_x \Delta_M^{-1}$ and $D_y \Delta_M^{-1}$ have zeros on the diagonal.

Let us write the discretizations J_0, J_E and J_Z as functions of $\boldsymbol{q}$ only

$$J_0(\boldsymbol{q}) = (D_x \boldsymbol{q}) * (D_y \Delta_M^{-1} \boldsymbol{q}) - (D_y \boldsymbol{q}) * (D_x \Delta_M^{-1} \boldsymbol{q}), \tag{3.11}$$

$$J_E(\boldsymbol{q}) = D_x(\boldsymbol{q} * D_y \Delta_M^{-1} \boldsymbol{q}) - D_y(\boldsymbol{q} * D_x \Delta_M^{-1} \boldsymbol{q}), \tag{3.12}$$

$$J_Z(\boldsymbol{q}) = D_y\left((D_x \boldsymbol{q}) * \Delta_M^{-1} \boldsymbol{q}\right) - D_x\left((D_y \boldsymbol{q}) * \Delta_M^{-1} \boldsymbol{q}\right). \tag{3.13}$$

We calculate, for (3.11),

$$\operatorname{div} J_0(\boldsymbol{q}) = \operatorname{tr}\left(D(D_y \Delta_M^{-1} \boldsymbol{q}) D_x\right) + \operatorname{tr}\left(D(D_x \boldsymbol{q}) D_y \Delta_M^{-1}\right)$$
$$- \operatorname{tr}\left(D(D_x \Delta_M^{-1} \boldsymbol{q}) D_y\right) - \operatorname{tr}\left(D(D_y \boldsymbol{q}) D_x \Delta_M^{-1}\right) = 0, \quad (3.14)$$

since each term is the trace of the product of a diagonal matrix and a matrix with zero diagonal.

For (3.12),

$$\operatorname{div} J_E(\boldsymbol{q}) = \operatorname{tr}\left(D_x \left[D(\boldsymbol{q}) D_y \Delta_M^{-1} + D(D_y \Delta_M^{-1} \boldsymbol{q})\right]\right) - \operatorname{tr}\left(D_y \left[D(\boldsymbol{q}) D_x \Delta_M^{-1} + D(D_x \Delta_M^{-1} \boldsymbol{q})\right]\right)$$
$$= \operatorname{tr}(D(\boldsymbol{q})[D_y \Delta_M^{-1} D_x - D_x \Delta_M^{-1} D_y]) + \operatorname{tr}\left(D_x D(D_y \Delta_M^{-1} \boldsymbol{q}) - D_y D(D_x \Delta_M^{-1} \boldsymbol{q})\right)$$
$$= 0.$$

The term in brackets in the last expression is identically zero by symmetry considerations.

Similarly, for (3.13) we have

$$\operatorname{div} J_Z(\boldsymbol{q}) = \operatorname{tr}\left(D_y \left[D(\Delta_M^{-1} \boldsymbol{q}) D_x + D(D_x \boldsymbol{q}) \Delta_M^{-1}\right]\right) - \operatorname{tr}\left(D_x \left[D(\Delta_M^{-1} \boldsymbol{q}) D_y + D(D_x \boldsymbol{q}) \Delta_M^{-1}\right]\right)$$
$$= \operatorname{tr}\left(D(\Delta_M^{-1} \boldsymbol{q})[D_x D_y - D_y D_x]\right) + \operatorname{tr}\left(D(D_x \boldsymbol{q}) \Delta_M^{-1} D_y - D(D_y \boldsymbol{q}) \Delta_M^{-1} D_y\right) = 0.$$

Finally, J_{EZ} is divergence-free because it is a linear combination of divergence-free vector fields.

4. ENERGY-ENSTROPHY STATISTICAL THEORY

The equilibrium statistical mechanical theory for 2D ideal fluids was developed by Kraichnan [8], and Salmon et al. [21]. It is based on a finite truncation of the spectral decomposition of the equations of motion. Statistical predictions are obtained for the truncated system, and these are extended to the infinite dimensional limit.

In this paper we will adapt the analysis to the semi-discretizations outlined in the previous section. For the discretization J_{EZ}, which conserves both energy and enstrophy, the analysis is identical to the spectral case, so in the following we simply review the presentation of Majda & Wang [11].

As previously noted, semi-discretization of (2.1) using the bracket (3.10) yields a system of M^2 ordinary differential equations having the Liouville property and two first integrals that approximate the energy (3.7) and enstrophy (3.8). Due to the Liouville property, one can speak of transport of probability density functions by this semi-discrete flow, and consider equilibrium solutions to Liouville's equation. In particular, any normalized function of the two first integrals is an equilibrium distribution.

4.1 Mean field predictions

The equilibrium distribution of least bias maximizes entropy under the constraints imposed by conservation of energy and enstrophy. Let $\boldsymbol{X}$ parametrize the M^2 dimensional phase space; that is, each $\boldsymbol{X} \in \mathrm{R}^{M \times M}$ corresponds to a particular realization of the grid function (or discrete field) $\boldsymbol{q}$. A probability distribution $\rho : \mathrm{R}^{M \times M} \to \mathrm{R}$ on phase space satisfies

$$\rho(\boldsymbol{X}) \geq 0, \qquad \int_{\mathrm{R}^{M \times M}} \rho(\boldsymbol{X}) \, d\boldsymbol{X} = 1.$$

The least biased distribution maximizes the entropy functional

$$\mathcal{S}[\rho] = -\int_{\mathrm{R}^{M \times M}} \rho(\boldsymbol{X}) \log \rho(\boldsymbol{X}) \, d\boldsymbol{X} \tag{4.1}$$

under constraints on the ensemble averages of energy:

$$\mathcal{K}_E[\rho] = \int_{\mathrm{R}^{M \times M}} E_M(\boldsymbol{X}) \rho(\boldsymbol{X}) \, d\boldsymbol{X} - E_M^* = 0, \tag{4.2}$$

and enstrophy:

$$\mathcal{K}_Z[\rho] = \int_{\mathrm{R}^{M \times M}} Z_M(\boldsymbol{X}) \rho(\boldsymbol{X}) \, d\boldsymbol{X} - Z_M^* = 0, \tag{4.3}$$

where E_M^* and Z_M^* are prescribed values. Additionally, there is the implied constraint that ρ be a probability distribution, i.e.

$$\mathcal{N}[\rho] = \int_{\mathrm{R}^{M \times M}} \rho(\boldsymbol{X}) \, d\boldsymbol{X} - 1 = 0. \tag{4.4}$$

Using the method of Lagrange multipliers, one seeks

$$\rho^* = \arg \max_{\rho} \{ \mathcal{S}[\rho] + \lambda_0 \mathcal{N}[\rho] + \lambda_1 \mathcal{K}_E[\rho] + \lambda_2 \mathcal{K}_Z[\rho] \}$$

to maximize the functional in braces. subject to the constraints (4.2)–(4.4), where the λ_j can be chosen to ensure (4.2)–(4.4). For the maximizing distribution, the variational derivative of the

expression enclosed in braces above must vanish. The variational derivatives of (4.1)–(4.4) are

$$\frac{\delta \mathcal{S}}{\delta \rho} = -(1 + \log \rho),$$

$$\frac{\delta \mathcal{K}_E}{\delta \rho} = E_M,$$

$$\frac{\delta \mathcal{K}_Z}{\delta \rho} = Z_M,$$

$$\frac{\delta \mathcal{N}}{\delta \rho} = 1.$$

The maximizing distribution must therefore satisfy

$$-(1 + \log \rho^*) + \lambda_1 E_M + \lambda_2 Z_M + \lambda_0 = 0.$$

This equation can be solved for ρ^* to give the Gibbs-like distribution (i.e. $\mathcal{G} \equiv \rho^*$)

$$\mathcal{G}(\boldsymbol{X}) = C^{-1} \exp\left[-\alpha \left(Z_M(\boldsymbol{X}) + \mu E_M(\boldsymbol{X})\right)\right], \tag{4.5}$$

where C is the normalizing constant to ensure (4.4) and α and μ are chosen to ensure (4.2) and (4.3).

The expected value of a function $F(\boldsymbol{X})$ is the ensemble average of F with the measure $\mathcal{G}$, denoted

$$\langle F \rangle = \int_{\mathrm{R}^{M \times M}} F(\boldsymbol{X}) \mathcal{G}(\boldsymbol{X}) \, d\boldsymbol{X}.$$

The mean state is obtained from the observation

$$\left\langle \frac{\partial Z_M}{\partial \boldsymbol{X}} + \mu \frac{\partial E_M}{\partial \boldsymbol{X}} \right\rangle = \int_{\mathrm{R}^{M \times M}} \left(\frac{\partial Z_M}{\partial \boldsymbol{X}} + \mu \frac{\partial E_M}{\partial \boldsymbol{X}} \right) C^{-1} \exp\left[-\alpha \left(Z_M(\boldsymbol{X}) + \mu E_M(\boldsymbol{X})\right)\right] d\boldsymbol{X}$$

$$= -\alpha^{-1} \int_{\mathrm{R}^{M \times M}} \frac{\partial}{\partial \boldsymbol{X}} \mathcal{G}(\boldsymbol{X}) \, d\boldsymbol{X} = 0$$

assuming $\mathcal{G}$ decays sufficiently fast at infinity. Since $\nabla_{\boldsymbol{q}} E_M = -\boldsymbol{\psi}$ and $\nabla_{\boldsymbol{q}} Z_M = \boldsymbol{q}$, the mean field relation

$$\langle \boldsymbol{q} \rangle = \mu \langle \boldsymbol{\psi} \rangle \tag{4.6}$$

follows. In other words, the ensemble averages of potential vorticity and stream function are linearly related. Coupled with the second relation of (2.1) one has

$$\Delta_M \langle \boldsymbol{\psi} \rangle = \langle \boldsymbol{q} \rangle - \boldsymbol{h},$$

which yields a modified Helmholtz problem for the stream function given μ:

$$(\mu - \Delta_M)\langle \boldsymbol{\psi} \rangle = \boldsymbol{h}. \tag{4.7}$$

4.2 PV fluctuation predictions
Majda & Wang [11] show that states (4.6) are nonlinearly stable steady states of (2.1). They rewrite solutions to (2.1) as the sum of mean and fluctuation parts

$$\boldsymbol{q} = \langle \boldsymbol{q} \rangle + \boldsymbol{q}', \qquad \boldsymbol{\psi} = \langle \boldsymbol{\psi} \rangle + \boldsymbol{\psi}', \qquad \langle \boldsymbol{q} \rangle = \mu \langle \boldsymbol{\psi} \rangle.$$

This yields the equation for fluctuations

$$\boldsymbol{q}'_t = J(\langle \boldsymbol{q} \rangle, \boldsymbol{\psi}') + J(\boldsymbol{q}', \langle \boldsymbol{\psi} \rangle) + J(\boldsymbol{q}', \boldsymbol{\psi}'), \qquad \Delta_M \boldsymbol{\psi}' = \boldsymbol{q}'. \tag{4.8}$$

This differential equation has the first integral

$$I_M(\boldsymbol{q}') \equiv Z'_M + \mu E'_M, \qquad Z'_M = \frac{1}{2}(\boldsymbol{q}')^T \boldsymbol{q}' \Delta x \Delta y, \quad E'_M = -\frac{1}{2}(\boldsymbol{\psi}')^T \boldsymbol{q}' \Delta x \Delta y. \tag{4.9}$$

One can also set up a statistical mechanics for the fluctuation equations and obtain predictions. To do so, let

$$\hat{p}_{\boldsymbol{k}} = \left(1 + \frac{\mu}{|\boldsymbol{k}|^2}\right)^{1/2} \hat{q}'_{\boldsymbol{k}}. \tag{4.10}$$

Then the Fourier transform of (4.9) gives

$$I_M = \frac{1}{2}\sum_{\boldsymbol{k}}\left(1 + \frac{\mu}{|\boldsymbol{k}|^2}\right)|\hat{q}'_{\boldsymbol{k}}|^2 \Delta x \Delta y = \frac{1}{2}\sum_{\boldsymbol{k}}|\hat{p}_{\boldsymbol{k}}|^2 \Delta x \Delta y = \frac{1}{2}\sum_{\boldsymbol{m}}p_{\boldsymbol{m}}^2 \Delta x \Delta y, \tag{4.11}$$

with corresponding fluctuation Gibbs distribution

$$\mathcal{G}'(\boldsymbol{p}) = C^{-1}\exp\left(-\frac{\beta}{2}\sum_{\boldsymbol{m}}p_{\boldsymbol{m}}^2 \Delta x \Delta y\right) = \prod_{\boldsymbol{m}}c^{-1}\exp\left(-\frac{\beta}{2}p_{\boldsymbol{m}}^2 \Delta x \Delta y\right), \tag{4.12}$$

where $c^{-M^2} = C^{-1}$. Denote the Guassian distribution with mean $\bar{x}$ and standard deviation σ by

$$g(x; \bar{x}, \sigma) = \frac{1}{\sigma\sqrt{2\pi}}\exp\left(-\frac{(x - \bar{x})^2}{2\sigma^2}\right),$$

for which it holds that $\int_{\mathrm{R}} g(x)\,dx = 1$. The distribution (4.12) is the product of M^2 identical such functions, i.e.,

$$\mathcal{G}'(\boldsymbol{p}) = \prod_{\boldsymbol{m}} g(p_{\boldsymbol{m}}; 0, \sigma_p),$$

where $\sigma_p = (\beta \Delta x \Delta y)^{-1/2}$.

Define the partial energy $I_{\boldsymbol{m}} = \frac{1}{2}p_{\boldsymbol{m}}^2 \Delta x \Delta y$. We calculate

$$\langle I_{\boldsymbol{m}}\rangle = \int_{\mathrm{R}^{M \times M}} \frac{1}{2}p_{\boldsymbol{m}}^2 \Delta x \Delta y \prod_{\boldsymbol{k}} g(p_{\boldsymbol{k}}; 0, \sigma_p)\,dp_{\boldsymbol{k}}$$

$$= \frac{\Delta x \Delta y}{2}\int_{\mathrm{R}} p_{\boldsymbol{m}}^2 g(p_{\boldsymbol{m}}; 0, \sigma_p)\,dp_{\boldsymbol{m}} = \frac{\Delta x \Delta y}{2}\sigma_p^2 = \frac{1}{2\beta}.$$

This holds for each partial energy. The energy is equipartitioned, and

$$\langle I_M\rangle = \sum_{\boldsymbol{m}}\langle I_{\boldsymbol{m}}\rangle = \sum_{\boldsymbol{m}}\frac{1}{2\beta} = \frac{M^2}{2\beta},$$

from which we obtain the estimates

$$\beta = \frac{M^2}{2\langle I_M\rangle}, \qquad \sigma_p = \sqrt{\frac{2\langle I_M\rangle}{M^2 \Delta x \Delta y}} = \sqrt{\frac{\langle I_M\rangle}{2\pi^2}}.$$

Let us further assume that the $p_{\boldsymbol{m}}$ are independent. Let $P = \boldsymbol{a}^T \boldsymbol{p}$ denote a linear combination of the $p_{\boldsymbol{m}}$. Since these are identically distributed, P is Gaussian with variation

$$\sigma(P)^2 = \boldsymbol{a}^T \boldsymbol{a}\sigma_p^2 = |\boldsymbol{a}|^2 \sigma_p^2.$$

From (4.10) we have

$$\boldsymbol{q}' = \mathcal{F}^{-1} \operatorname{diag}\left(\left(1 + \frac{\mu}{|\boldsymbol{k}|^2}\right)^{-1/2} \right) \mathcal{F} \boldsymbol{p} = A\boldsymbol{p},$$

where A is real and symmetric. It follows that the time series $q'_{\boldsymbol{m}}(t)$ at each grid point $\boldsymbol{m}$ is Gaussian with mean zero and variance

$$\sigma_q^2 = |\boldsymbol{a}|^2 \sigma_p^2 = |\boldsymbol{a}|^2 \frac{\langle I_M \rangle}{2\pi^2}, \tag{4.13}$$

where for $\boldsymbol{a}$ we can take any row of A.

4.3 Approximation of μ and α

The ensemble averages of energy and enstrophy can be split into a mean part and a fluctuation part [11]:

$$\langle E_M \rangle = E_M(\langle \boldsymbol{q} \rangle) + E'_M, \qquad \langle Z_M \rangle = Z_M(\langle \boldsymbol{q} \rangle) + Z'_M, \tag{4.14}$$

where, using (4.7),

$$E_M(\langle \boldsymbol{q} \rangle) = -\frac{1}{2}\langle \boldsymbol{\psi} \rangle^T (\langle \boldsymbol{q} \rangle - \boldsymbol{h}) \Delta x \Delta y = \frac{1}{2} \sum_{k_1,k_2=-M/2+1}^{M/2} \frac{|\boldsymbol{k}|^2 |\hat{h}_{\boldsymbol{k}}|^2}{(\mu + |\boldsymbol{k}|^2)^2} \Delta x \Delta y, \tag{4.15a}$$

$$E'_M = \frac{1}{2\alpha} \sum_{k_1,k_2=-M/2+1}^{M/2} \frac{1}{\mu + |\boldsymbol{k}|^2}, \tag{4.15b}$$

and

$$Z_M(\langle \boldsymbol{q} \rangle) = \frac{1}{2}\langle \boldsymbol{q} \rangle^T \langle \boldsymbol{q} \rangle \Delta x \Delta y = \frac{1}{2} \sum_{k_1,k_2=-M/2+1}^{M/2} \frac{\mu^2 |\hat{h}_{\boldsymbol{k}}|^2}{(\mu + |\boldsymbol{k}|^2)^2} \Delta x \Delta y, \tag{4.16a}$$

$$Z'_M = \frac{1}{2\alpha} \sum_{k_1,k_2=-M/2+1}^{M/2} \frac{|\boldsymbol{k}|^2}{\mu + |\boldsymbol{k}|^2}. \tag{4.16b}$$

Given guesses for μ and α, it is straightforward to compute $\langle E_M \rangle$ and $\langle Z_M \rangle$ by solving (4.15) and (4.16) and then substituting into (4.14). To estimate μ and α, we proceed iteratively, by implicitly solving (4.2) and (4.3) under that assumptions $E_M^* \approx \mathcal{E}_0$ and $Z_M^* \approx \mathcal{Z}_0$.

4.4 Alternative statistical theories

In this section we derive alternative statistical models for the cases where either energy or enstrophy, but not both, is conserved numerically.

4.4.1 Energy-based statistical mechanics
For a semi-discretization that only preserves the energy E_M, the least biased distribution (4.5) becomes

$$\mathcal{G}_E(\boldsymbol{X}) = C^{-1} \exp\left\{ -\lambda E_M(\boldsymbol{X}) \right\}.$$

The mean field prediction (4.6) gives

$$\langle \boldsymbol{\psi} \rangle \equiv 0, \qquad \langle \boldsymbol{q} \rangle = \boldsymbol{h}. \tag{4.17}$$

The fluctuation dynamics (4.8) becomes

$$\boldsymbol{q}'_t = J_E(\boldsymbol{h} + \boldsymbol{q}', \boldsymbol{\psi}'), \qquad \boldsymbol{\psi}' = \Delta_M^{-1} \boldsymbol{q}',$$

which preserves the pseudo-energy

$$I_M = -\frac{1}{2}(\boldsymbol{\psi}')^T \boldsymbol{q}' \Delta x \Delta y = E_M' \approx \mathcal{E}_0$$

We define

$$\hat{p}_{\boldsymbol{k}} = \frac{\hat{q}_{\boldsymbol{k}}'}{(|\boldsymbol{k}|^2)^{1/2}},$$

and obtain the fluctuation Gibbs distribution (4.12) with $\sigma_p = (\langle I_M \rangle / 2\pi^2)^{1/2}$. The fluctuation vorticity σ_q is given by (4.13) with $A = (-\Delta_M)^{1/2}$.

4.4.2 Enstrophy-based statistical mechanics   For a semi-discretization that only preserves the enstrophy Z_M, the least biased distribution (4.5) becomes

$$\mathcal{G}_E(\boldsymbol{X}) = C^{-1} \exp\{-\lambda Z_M(\boldsymbol{X})\}.$$

The mean field prediction (4.6) gives

$$\langle \boldsymbol{q} \rangle \equiv 0, \qquad \langle \boldsymbol{\psi} \rangle = -\Delta_M^{-1} \boldsymbol{h}. \tag{4.18}$$

The fluctuation dynamics (4.8) becomes

$$\boldsymbol{q}' = J_Z(\boldsymbol{q}', \langle \boldsymbol{\psi} \rangle + \boldsymbol{\psi}'), \qquad \boldsymbol{\psi}' = \Delta_M^{-1} \boldsymbol{q}',$$

and the pseudo-energy is just the enstrophy, i.e.

$$I_M = \frac{1}{2}(\boldsymbol{q}')^T \boldsymbol{q}' \Delta x \Delta y = Z_M' \approx \mathcal{Z}_0.$$

We obtain the fluctuation Gibbs distribution (4.12) with $\hat{p}_{\boldsymbol{k}} = \hat{q}_{\boldsymbol{k}}'$ and find

$$\sigma_q = \sqrt{\frac{\langle I_M \rangle}{2\pi^2}}.$$

5. TIME INTEGRATION
5.1 *Time discretizations*
Since both invariants E_M and Z_M of the discretizations are quadratic functions of $\boldsymbol{q}$, they are automatically conserved if the equations are integrated with a Gauss-Legendre Runge-Kutta method [6]. The simplest such method is the implicit midpoint rule

$$\frac{\boldsymbol{q}^{n+1} - \boldsymbol{q}^n}{\Delta t} = J\left(\frac{\boldsymbol{q}^{n+1} + \boldsymbol{q}^n}{2}, \frac{\boldsymbol{\psi}^{n+1} + \boldsymbol{\psi}^n}{2}\right).$$

The discretization is also symmetric, and in the case of zero topography $h(\boldsymbol{x}) \equiv 0$, preserves the time reversal symmetry $t \mapsto -t$, $q \mapsto -q$ of (2.1). Although it is symplectic for Hamiltonian systems with constant structure operators, the implicit midpoint rule is not volume preserving in general. Indeed, a numerical check indicates that it does not preserve volume for our discretizations. However, it is nondamping and exactly preserves linear stability, and, as our numerical experiments indicate, it does accurately reproduce the statistical predictions, even for a relatively large step size.

Implicit midpoint requires the solution of a nonlinear system of dimension M^2 at every time step. As a more efficient alternative, we can take any explicit Runge-Kutta method and project the solution onto the integral manifolds as desired. Let the Runge-Kutta method be represented by a map $\boldsymbol{q}^{n+1} = \Phi_{\Delta t}(\boldsymbol{q}^n)$ and compute a predicted step

$$\boldsymbol{q}^* = \Phi_{\Delta t}(\boldsymbol{q}^n).$$

Then project $\boldsymbol{q}^*$ onto the desired constraint manifolds. For example, we solve

$$\boldsymbol{q}^{n+1} = \boldsymbol{q}^* + \boldsymbol{g}'(\boldsymbol{q}^*)^T \boldsymbol{\lambda}$$
$$\boldsymbol{g}(\boldsymbol{q}^{n+1}) = 0$$

for $\boldsymbol{\lambda}$ where $\boldsymbol{g}(\boldsymbol{q}) : \mathrm{R}^{M \times M} \to \mathrm{R}^r$, r the number of first integrals, and $\boldsymbol{\lambda} \in \mathrm{R}^r$ is a vector of Lagrange multipliers. For example, we can take $(r = 3)$

$$\boldsymbol{g}(\boldsymbol{q}) = \begin{pmatrix} E_M(\boldsymbol{q}) - \mathcal{E}_0 \\ Z_M(\boldsymbol{q}) - \mathcal{Z}_0 \\ (\sum_{\boldsymbol{m}} q_{\boldsymbol{m}}) - 1 \end{pmatrix},$$

where the last constraint ensures that there is no drift in total vorticity. At each time step, projection requires solving a small nonlinear problem of dimension r. Projected Runge-Kutta methods will generally not preserve volume.

One can also combine projection with an arbitrary spatial discretization, i.e. even one that does not have E_M or Z_M as a first integral. This allows us to investigate the relative importance of conservation in spatial and temporal discretizations. In the numerical experiments we use J_0, for which we have established that the semi-discretization preserves volume but neither energy nor enstrophy.

5.2 Time averages

Our interest is in the statistics applied to numerical data obtained from simulations over long times. To apply the theory from the previous sections, we further have to assume that the semi-discrete dynamics are ergodic. Denote the time average of a quantity $F(\boldsymbol{q}(t))$ by

$$\bar{F}_T = \frac{1}{T} \int_{t_0}^{t_0+T} F(\boldsymbol{q}(t)) \, dt.$$

Then the assumption of ergodicity implies that the long time average converges to the ensemble average

$$\bar{F} = \lim_{T \to \infty} \bar{F}_T = \langle F \rangle.$$

On the other hand, suppose one chooses discrete initial conditions to have a prescribed energy and enstrophy consistent with the continuum problem, i.e.

$$E_M(\boldsymbol{q}(0)) = \mathcal{E}_0, \qquad Z_M(\boldsymbol{q}(0)) = \mathcal{Z}_0.$$

Then it is clear that since $E_M(\boldsymbol{q}(t)) = E_M(\boldsymbol{q}(0))$ and $Z_M(\boldsymbol{q}(t)) = Z_M(\boldsymbol{q}(0))$ are conserved, the dynamics only samples at best a codimension two subspace of $\mathrm{R}^{M \times M}$, so one may ask to what extent the averages will converge. Indeed, one has inequality

$$\bar{E}_M = \langle E_M \rangle \neq \mathcal{E}_0, \qquad \bar{Z}_M = \langle Z_M \rangle \neq \mathcal{Z}_0,$$

in general. By analogy with molecular dynamics, the Gibbs distribution (4.5) determines expectations in the canonical ensemble, whereas a constant energy-enstrophy simulation determines expectations in the microcanonical ensemble (assuming ergodicity). It is only in the 'thermodynamic limit' $M \to \infty$ that these averages coincide, giving equality in the above relations.

6. NUMERICAL EXPERIMENTS

For the numerical experiments we use the test problem of [1]. The grid resolution is $M = 22$. The orography is a function of x only, specifically

$$h(x, y) = 0.2 \cos x + 0.4 \cos 2x.$$

(As a result the predicted mean fields $\bar{q}$ and $\bar{\psi}$ should be functions of x only.) The integrations were carried out using a step size of $\Delta t = 0.1$.

For initial conditions we take a random field[1] $q = q_{m_1,m_2}$, $m_1, m_2 = 1, \ldots M$ and project this onto the constraints

$$E_M(q) = \mathcal{E}_0, \quad Z_M(q) = \mathcal{Z}_0, \quad \sum_m q_m = 0.$$

The same initial condition is used for all simulations. The discrete energy and enstrophy were taken to be $\mathcal{E}_0 = 7$ and $\mathcal{Z}_0 = 20$.

With these values prescribed, the statistical predictions of Section 4 can be computed for the three discretizations (3.5), (3.6), and (3.10). The Lagrange multiplier μ is computed using the procedure described at the end of Section 4.3. Fluctuation statistics apply to the time series of PV at an arbitrarily chosen monitor point on the grid $q_{\text{mon}} = q_{3,12}$.

For the energy-enstrophy theory we obtain the mean state (4.6) and estimates

$$J_{EZ}: \quad \mu = -0.730, \qquad \langle q_{\text{mon}} \rangle = -0.341, \qquad \sigma_q = 0.970. \tag{6.1}$$

For the energy theory of Section 4.4.1 we obtain the mean state (4.17) and estimates

$$J_E: \quad \langle \psi \rangle \equiv 0, \qquad \langle q_{\text{mon}} \rangle = 0.0740, \qquad \sigma_q = 5.36. \tag{6.2}$$

For the enstrophy theory of Section 4.4.2 we obtain the mean state (4.18) and estimates

$$J_Z: \quad \mu = 0, \qquad \langle q_{\text{mon}} \rangle = 0, \qquad \sigma_q = 1.01. \tag{6.3}$$

6.1 Results using implicit midpoint

We first present results obtained using the implicit midpoint discretization in time. The nonlinear relations were solved using fixed point iteration to a tolerance of 10^{-13}, which was the smallest tolerance that gave convergence at each step size for all discretizations. The solutions were averaged over the interval $[10^3, T]$, for $T = 10^4$, 10^5 and 10^6.

Given the average fields $\bar{q}$ and $\bar{\psi}$, the best linear fit to (4.6) yields an estimate of the Lagrange multiplier μ, i.e.

$$\bar{\mu} = \frac{\bar{\psi}^T \bar{q}}{\bar{\psi}^T \bar{\psi}}.$$

The relative change in energy and enstrophy for each discretization is plotted in Figure 1 on the interval $[0, 10^4]$. The relative change is defined as

$$\Delta E_M^n = \frac{E_M^n - \mathcal{E}_0}{\mathcal{E}_0}, \qquad \Delta Z_M^n = \frac{Z_M^n - \mathcal{Z}_0}{\mathcal{Z}_0}.$$

For the discretization J_{EZ}, both quantities are conserved up to the tolerance of the fixed point iteration, which leads to a small drift of magnitude 3×10^{-11} (relative) over this interval. For the J_E discretization, energy is conserved to the tolerance of the fixed point iteration, but enstrophy makes a rapid jump to a mean state roughly 30 times its initial value and subsequently undergoes bounded fluctuations with amplitude about 10 times Z_0. By contrast, for the J_Z discretization, enstrophy is similarly conserved, but energy drifts gradually with a negative trend, by about 30% of its initial value.

6.1.1 Long-time mean fields The time-averaged mean field $\bar{\psi}$ obtained by averaging over the interval $[10^3, 10^4]$ is shown in Figure 2 for the three discretizations J_{EZ}, J_E and J_Z. Also shown is a scatter plot of the locus $(\bar{\psi}_m, \bar{q}_m)$ and a linear best fit to this data for the respective discretizations. For the J_{EZ} discretization, the mean stream function is similar to that predicted by the energy-enstrophy statistical theory (4.6), with $\bar{\mu} = -0.734$. For the J_E discretization, the mean stream function satisfies $\bar{\psi} \approx 0$, consistent with (4.17), and the linear regression is inaccurate. For the J_Z
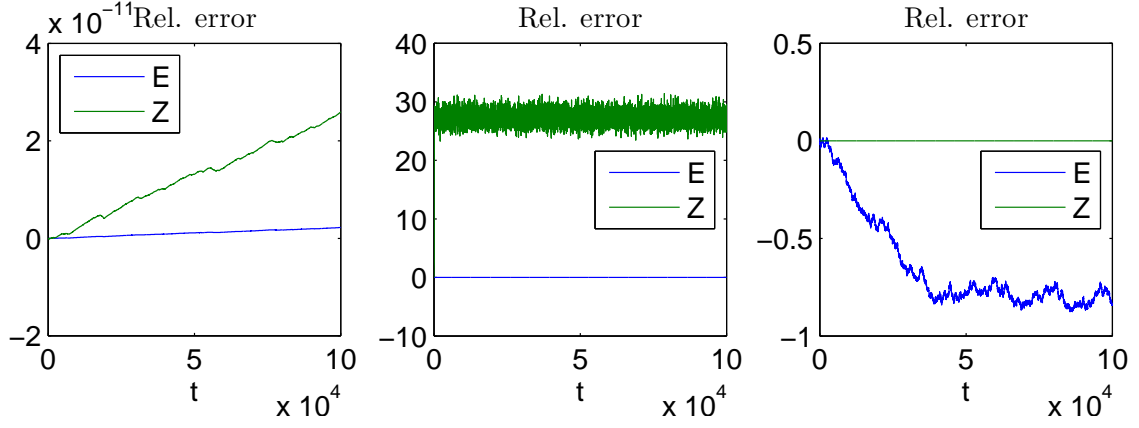
Figure 1: Relative change in energy and enstrophy with discretizations J_{EZ} (left), J_E (middle), and J_Z (right).
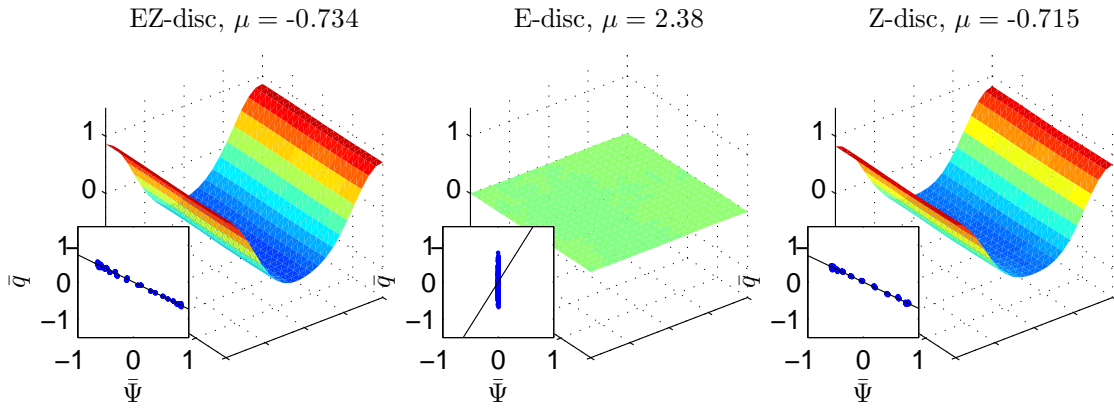
Figure 2: Mean fields with averaging time 10^4, J_{EZ} (left), J_E (middle), and J_Z (right). The insets show the best linear fit to the relation $\bar{\psi}_{\boldsymbol{m}} = \mu \bar{q}_{\boldsymbol{m}}$ at all grid points.

discretization, we observe a similar mean state with $\bar{\mu} = -0.715$ on this averaging interval, which is inconsistent with prediction (6.3).

In Figures 3 and 4 we examine more closely the mean fields for the J_{EZ} and J_Z discretizations, for longer averaging times of $T = 10^5$ and $T = 10^6$. For the energy-enstrophy discretization J_{EZ} in Figure 3, the mean field appears to converge to an equilibrium state with $\bar{\mu} \approx -0.732$. The tendency in Figure 4 is toward a mean field with zero vorticity, consistent with (4.18). However the relaxation time is much longer than for the other discretizations. For $T = 10^6$, the mean flow has $\bar{\mu} = -0.0529$. Note that the relation $\bar{q} = \mu\bar{\psi}$ approximates the data well, however. In Section 6.1.3 below, we show that the convergence of the J_Z discretization is in agreement with the J_{EZ} predictions on short time intervals, so that we can think of the system staying near statistical equilibrium with slowly drifting energy.
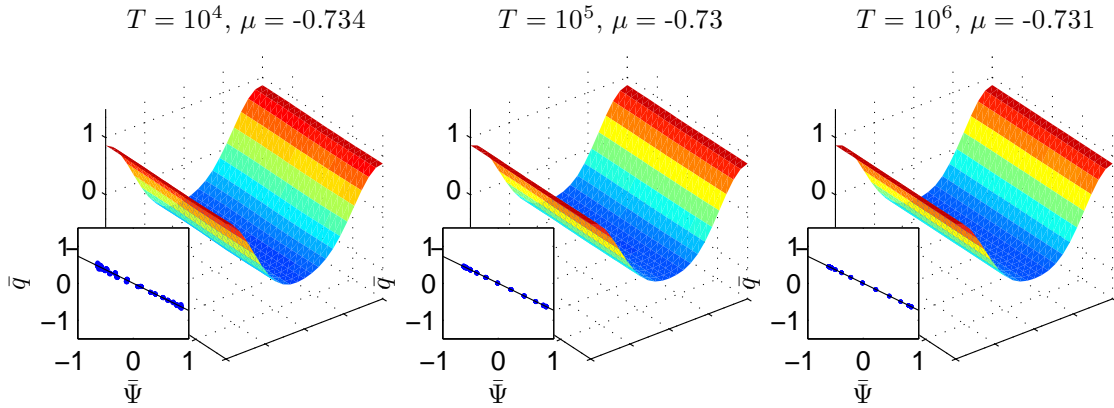
Figure 3: Mean fields for discretization J_{EZ} with averaging times 10^4 (left), 10^5 (middle), and 10^6 (right). The insets show the best linear fit to the relation $\bar{\psi}_{\boldsymbol{m}} = \mu\bar{q}_{\boldsymbol{m}}$ at all grid points.
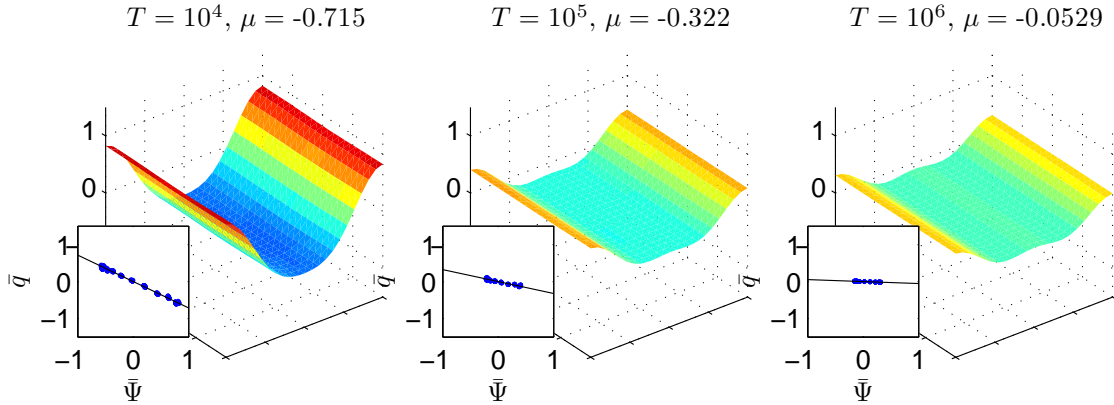
Figure 4: Mean fields for discretization J_Z with averaging times 10^4 (left), 10^5 (middle), and 10^6 (right). The insets show the best linear fit to the relation $\bar{\psi}_{\boldsymbol{m}} = \mu\bar{q}_{\boldsymbol{m}}$ at all grid points.

6.1.2 PV fluctuation statistics In Figure 5, the time series for potential vorticity q_{mon} at an arbitrarily chosen grid point $(3, 12)$ is analyzed. As discussed in Section 4.2, the statistical theory for fluctuations predicts that the PV should be distributed normally about the mean field according to (6.1)–(6.3). For the longest simulation time of $T = 10^6$, the J_{EZ} discretization exhibits Gaussian

---

[1]Experiments with smooth initial conditions show no noticable difference.

fluctuations with mean $\bar{q}_{\mathrm{mon}} = -0.395$ and standard deviation $\sigma = 0.927$; the J_E discretization with mean $\bar{q}_{\mathrm{mon}} = -0.0093$ and standard deviation $\sigma = 5.35$; and the J_Z discretization with mean $\bar{q}_{\mathrm{mon}} = -0.0575$ and standard deviation $\sigma = 1.05$. These observations are approximately in agreement with (6.1)–(6.3).

We mention that the value $\bar{m}u = 0.732$, to which the J_{EZ} discretization seems to relax, corresponds to a mean energy value of $\langle E_N \rangle = 7.07$. For this value of mean energy, the prediction of Section 4.2 gives $\sigma = 0.928$, which is much closer to the value observed in Figure 5. This indicates that for implicit midpoint, the mean energy is somewhat preturbed from the microcanonical energy $\mathcal{E}_0$.
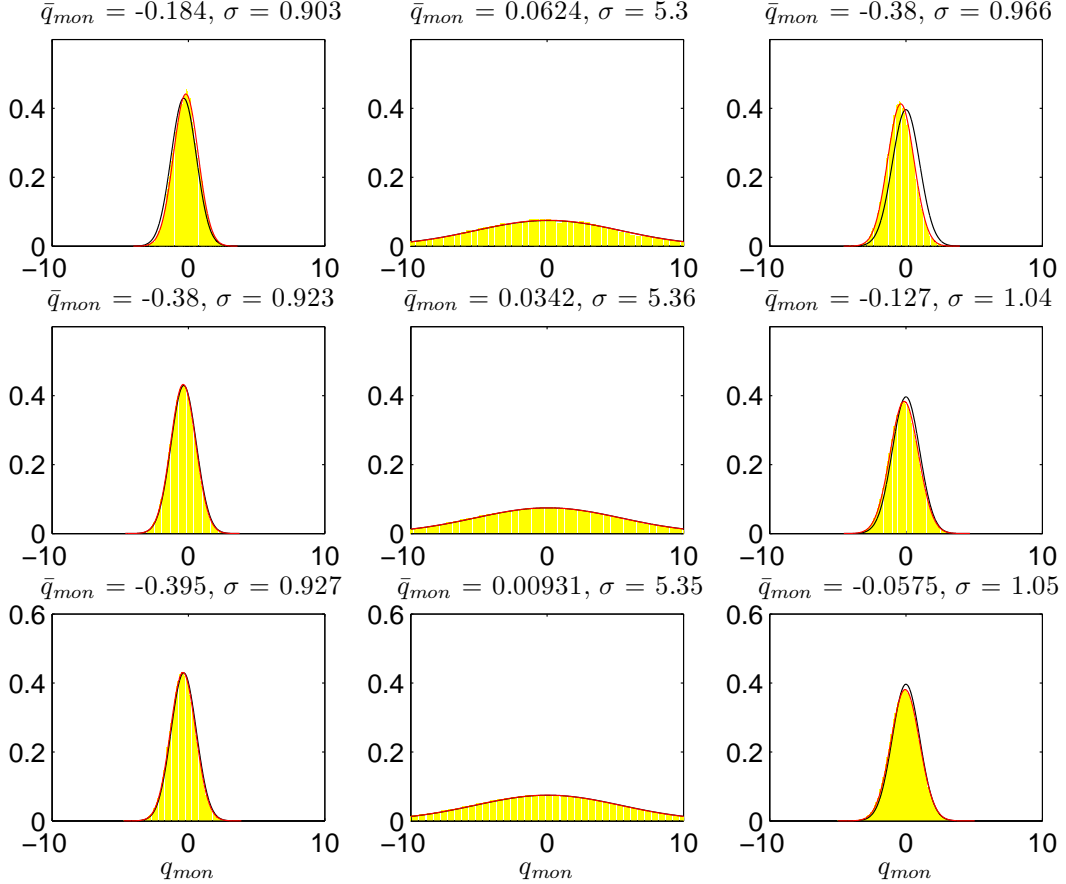
Figure 5: Fluctuation statistics for the potential vorticity about the predicted mean. The histogram is observation. The red line is a Gaussian fit. The black line is the predicted distribution. Discretizations J_{EZ}, J_E, and J_Z in left, middle and right columns. Integration intervals of 10^4, 10^5 and 10^6 in top, middle and bottom rows.

6.1.3 Time-dependent energy-enstrophy model   In Figure 6, the convergence of $\bar{\mu}$ is plotted as a function of averaging interval T for both the J_Z and J_{EZ} discretizations. The J_{EZ} dynamics relaxes very rapidly to give $\bar{\mu} \approx -0.73$, whereas the J_Z dynamics converges rather slowly towards $\bar{\mu} = 0$. Given the relatively fast relaxation of the energy-enstrophy conserving discretization to statistical equilibrium (4.6) and the slow drift of energy in Figure 1 for the enstrophy conserving discretization J_Z, a natural model for the approach to equilibrium would be to consider a state $\bar{q}_T = \bar{\mu}_T \bar{\psi}_T$ with $\bar{\mu}_T$ corresponding to the instantaneous energy $E_M(T)$.

To test this idea, we define

$$\bar{\boldsymbol{\psi}}_T = \frac{1}{N_T} \sum_{n=1}^{N_T} \boldsymbol{\psi}^n, \qquad \bar{\boldsymbol{q}}_T = \frac{1}{N_T} \sum_{n=1}^{N_T} \boldsymbol{q}^n,$$

where $T = N_T \cdot \Delta t$, and

$$\mu_T = \frac{(\bar{\boldsymbol{\psi}}_T)^T \bar{\boldsymbol{q}}_T}{(\bar{\boldsymbol{\psi}}_T)^T \bar{\boldsymbol{\psi}}_T}.$$

The energy of the associated equilibrium state is denoted $E_M(\bar{\mu}_T)$ and is determined from the relations in Section 4.3. This energy is plotted in Figure 7 next to the actual discrete energy function, for increasing averaging intervals $T = 10$, $T = 100$ and $T = 1000$. The agreement supports this model. That is, the J_Z dynamics relaxes on a fast time scale to the statistical equilibrium predicted by energy-enstrophy theory *for the instantaneous energy*, while the energy drifts on a slow time scale towards the equilibrium state predicted by the enstrophy theory.
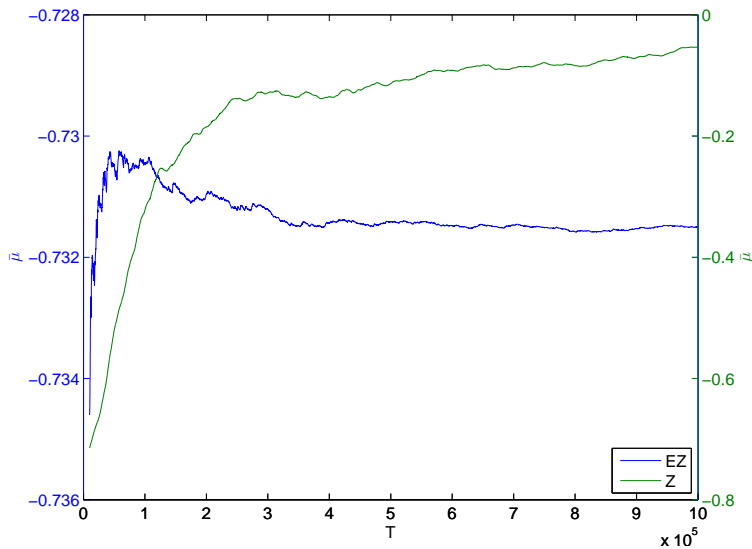
Figure 6: Convergence of parameter μ_T as a function of the averaging interval T for the J_{EZ} and J_Z discretizations.

6.2 Results using projected Heun's method

Besides preserving quadratic first integrals exactly, the implicit midpoint rule is symmetric. It is unclear what effect, if any, this may have on statistics. Furthermore, the implicit midpoint rule is fully implicit and therefore not a very practical choice for integrating a nonstiff system such as (2.1). For these reasons we repeat the experiments of the previous section using the second order, explicit Runge-Kutta method due to Heun [7], coupled with projection onto the discrete energy and/or enstrophy manifolds. It should be noted that Heun's method is linearly unstable with respect to a center equilibrium, and it is only due to projection that we can carry out long integrations with this method.

Figure 8 compares the convergence of the parameter $\bar{\mu}_T$ as a function of T for the implicit midpoint and projected Heun integrators for the J_{EZ} and J_Z discretizations. In both cases, it appears that the projected method approaches equilibrium faster than implicit midpoint.

Figures 9, 10 and 11 are analogous to Figures 2, 3 and 4 for implicit midpoint. Again we note that the projected method converges more rapidly and more accurately to the mean states (6.1)–(6.3). The fluctuation statistics for the projection method are illustrated in Figure 12. Here, too, we see that the projection method is very close to the statistically predicted value for mean and
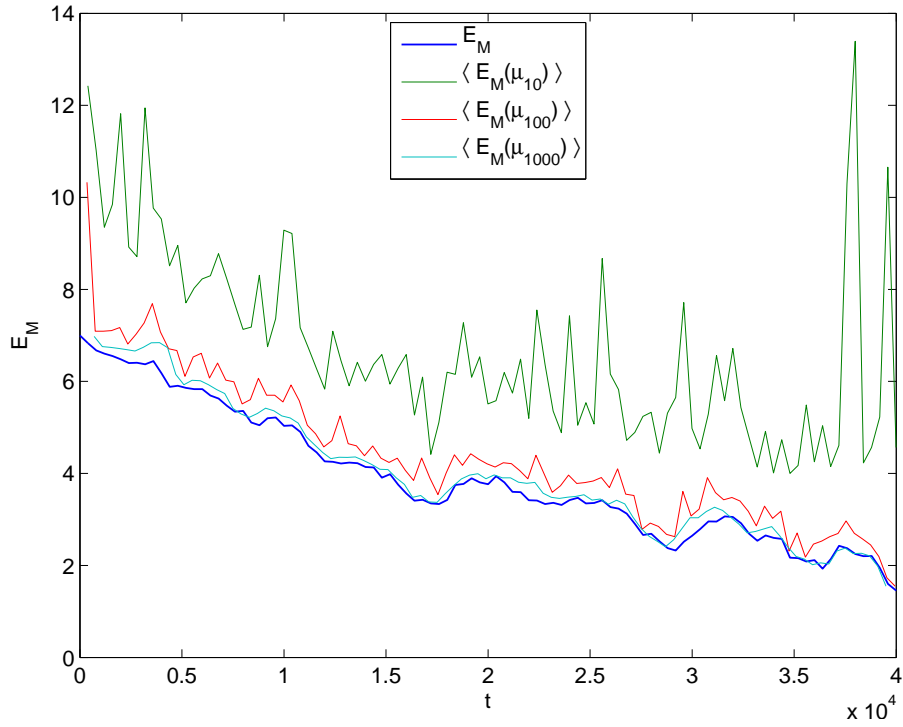
Figure 7: Energy drift with J_Z discretization, compared to the energy associated with the best linear fit μ_T with averaging intervals $T = 10$, $T = 100$ and $T = 1000$.
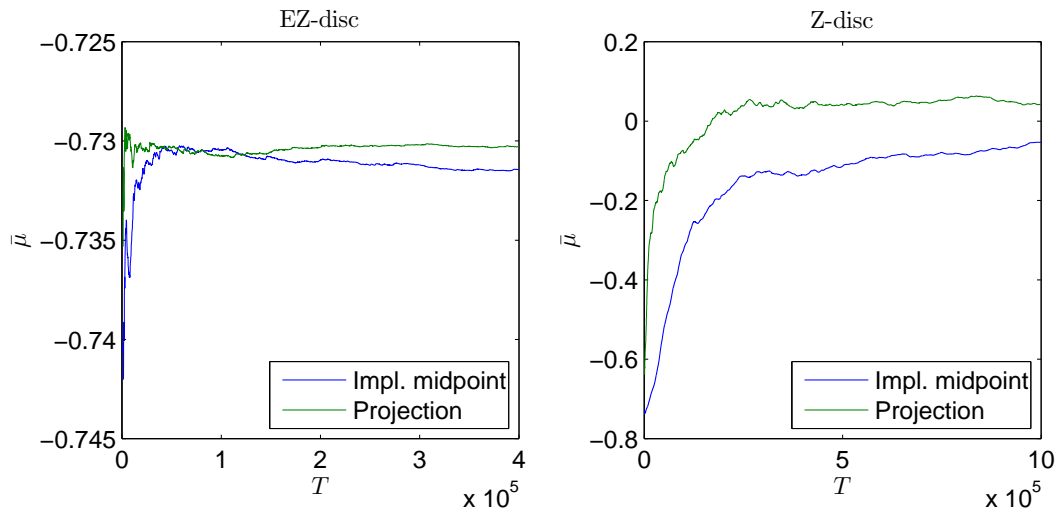
Figure 8: Convergence of μ_T as a function of averaging interval T for J_{EZ} (left) and J_Z (right) discretizations, comparing the projected Heun's method and implicit midpoint.

EZ-disc, μ = -0.731   E-disc, μ = -31.5   Z-disc, μ = -0.355
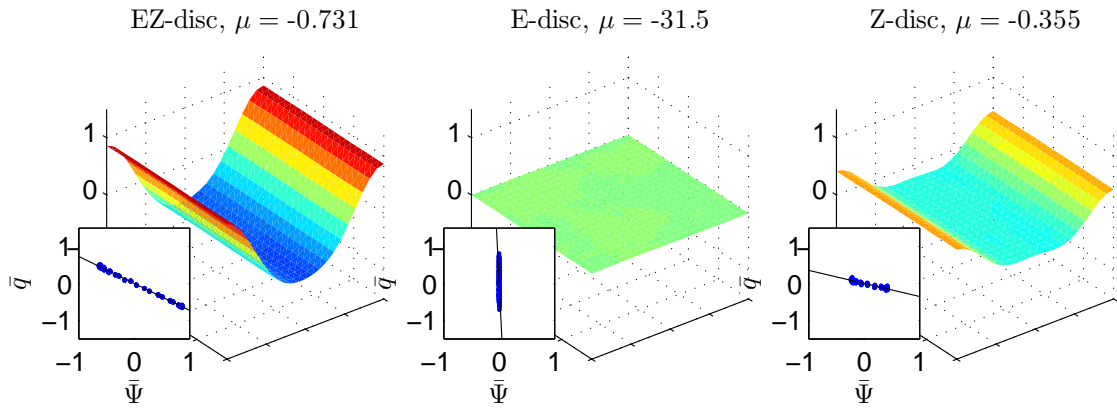
Figure 9: Same as Figure 2, but using projected Heun's method

$T = 10^4$, μ = -0.731 $T = 10^5$, μ = -0.731 $T = 10^6$, μ = -0.73
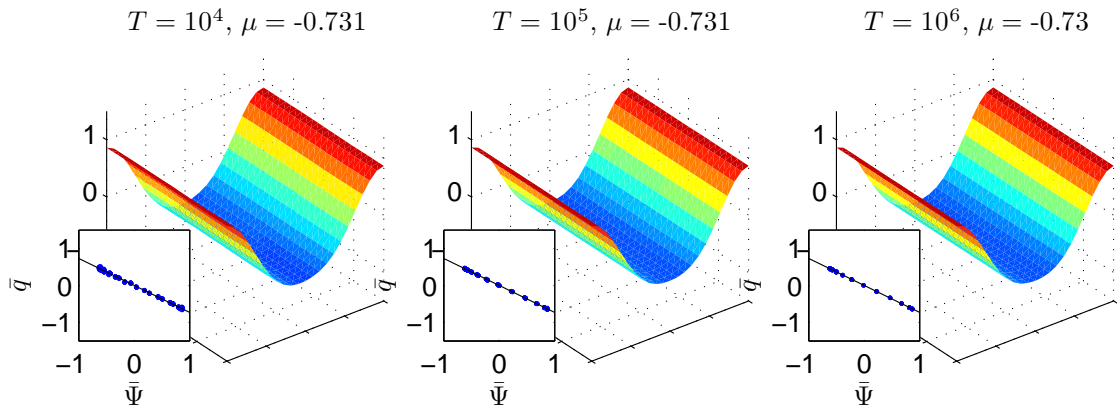
Figure 10: Same as Figure 3, but using projected Heun's method.

$T = 10^4$, μ = -0.355 $T = 10^5$, μ = -0.0799 $T = 10^6$, μ = 0.0423
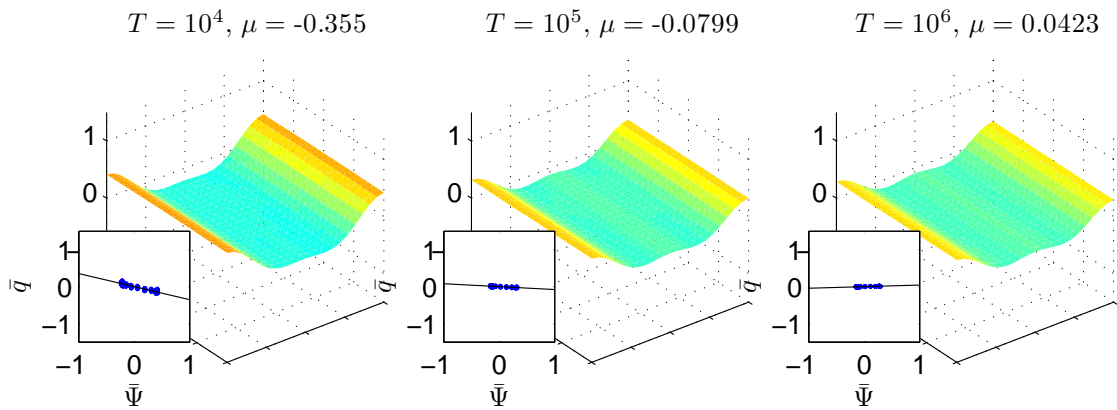
Figure 11: Same as Figure 4, but using projected Heun's method.

standard deviation of PV fluctuations in (6.1)–(6.3). However, it is important to note that since a measure of predictability is the *deviation from the statistical equilibrium*, a numerical method that approaches equilibrium excessively fast is undesirable from a prediction perspective.
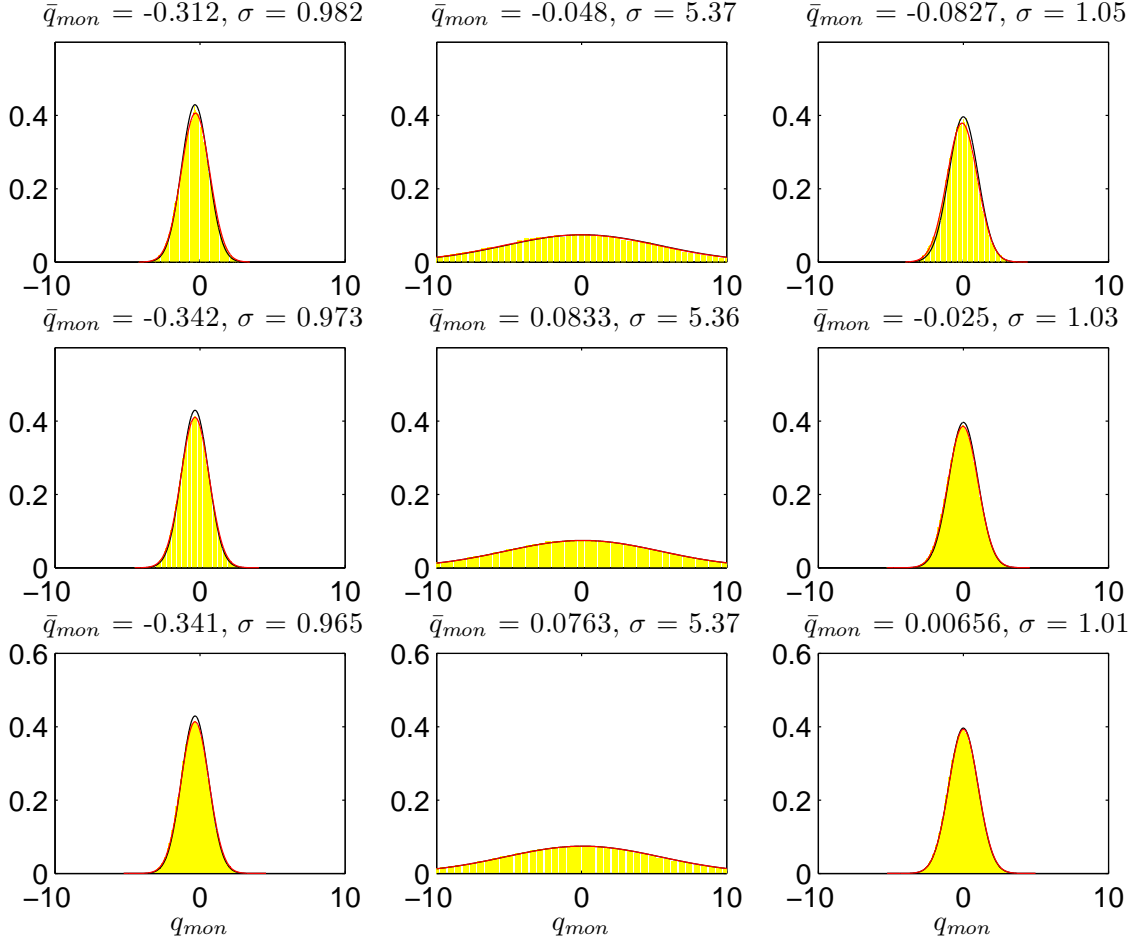
Figure 12: Same as Figure 5, but using projected Heun's method.

6.3 The importance of conservative spatial discretization

One may ask about the relative importance of the conservative properties of the spatial and temporal discretizations. We can project any solution onto the energy or enstrophy manifolds; is it really necessary that the spatial discretization have these quantities as first integrals? In this section we demonstrate numerically that the conservation properties of the spatial discretization are vital to obtaining correct statistics.

We repeat the experiment of the previous section, this time using the spatial discretization J_0 which conserves neither energy nor enstrophy. The semi-discretization is integrated in time with the projected Heun method of the previous section.

The numerical results are presented in Figures 13 and 14 for the intermediate averaging interval of $T = 10^5$. We note that the mean state (4.6) is still recovered accurately for projection on both energy and enstrophy. For projection on energy or enstrophy alone, however, the mean states do not agree with the statistical predictions (6.2) and (6.3). In all cases the fluctuation statistics are entirely incorrect. In fact, further experimentation suggests that in the absence of conservative structure in the semi-discretization, projection introduces an asymptotically stable limit cycle that attracts a large set of initial conditions.
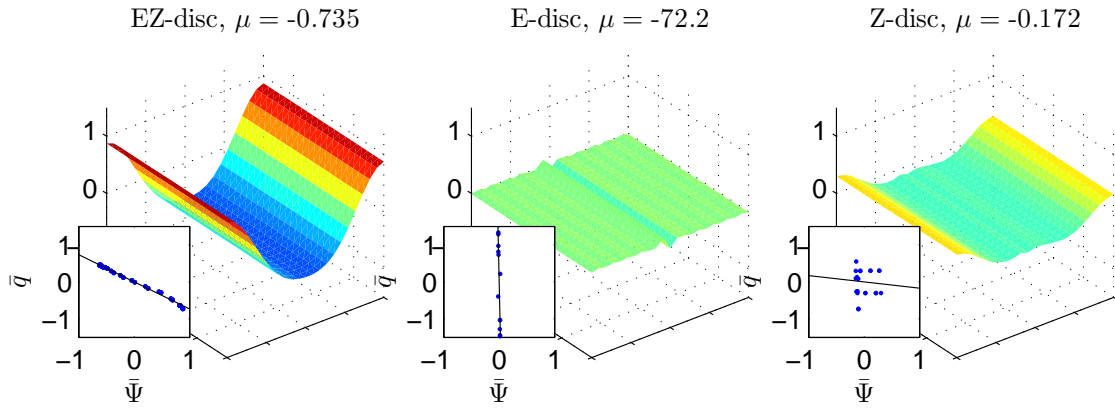
Figure 13: Same as Figure 2, but using semi-discretization J_0 and projected Heun's method, $T = 10^5$.
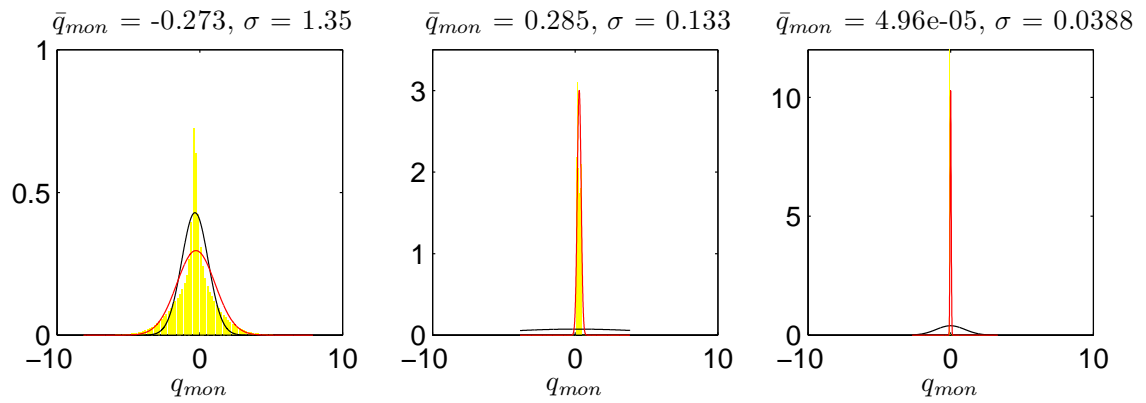
Figure 14: Same as the middle row of Figure 5, but using semi-discretization J_0 and projected Heun's method.

7. CONCLUSIONS

In this paper we have constructed statistical mechanical theories for three conservative discretizations of the quasi-geostrophic model due to Arakawa [2], based on conservation of energy, enstrophy, or both. Numerical experiments indicate that the statistical theories can give insight into the long time behavior of the discretizations, making this approach a useful tool for numerical analysis.

Time integration of the semi-discretization was done with the symmetric implicit midpoint method—which automatically conserves any quadratic first integrals of the semi-discrete system—and with a projected Runge-Kutta method. Long time averages with the implicit midpoint discretization relax to the predicted equilibrium at a slower rate than for the projected method, suggesting that implicit midpoint has higher potential for prediction.

Experiments with a nonconservative spatial discretization and projected time integrator show that the conservative properties of the spatial discretization are essential for statistical accuracy. A conservative spatial discretization ensures proper local transport of energy and/or enstrophy.

The three statistical theories predict dramatically different behavior, and this is confirmed by the numerical experiments. In other words, the three discretizations exhibit dramatically different behavior in simulations over long intervals. The statistical equilibrium states define a backdrop on which the discrete dynamics occurs, and that backdrop depends on the conservation properties of the spatial discretization. Assuming the energy-enstrophy theory to be correct, it is thus essential for any code to preserve both quantities (under semi-discretization) if statistical accuracy is desired. On the other hand, it has been shown by Abramov & Majda [1] that the energy-enstrophy theory is incomplete. In [1], the Poisson discretization of [25] is integrated using the Poisson splitting of McLachlan [13]. The semi-discretization preserves, in addition to the Hamiltonian, N Casimirs corresponding to the first N moments of potential vorticity (PV), and these are preserved by the splitting (the energy is only preserved approximately, in the sense of backward error analysis [6]). Abramov & Majda give convincing evidence that nonzero values of the third moment of PV, when conserved by the discretization, can significantly skew the predictions of the standard theory of [8, 21, 11].

Nonetheless the results of this paper make a strong argument for the use of conservative discretizations in weather and climate simulations.

Planned further work on the subjects of this paper will address shallow water equations on the sphere, energy and enstrophy conserving discretizations [22, 19, 20], and the Hamiltonian Particle-Mesh method [3, 4, 5], a symplectic discretization of inviscid fluids. In [4] it is shown that the HPM method satisfies a circulation theorem, but it is uncertain to what extent this can be interpreted as enstrophy conservation. We expect the current approach will clarify this issue.

REFERENCES

1. R. V. Abramov and A. J. Majda. Statistically relevant conserved quantities for truncated quasigeostrophic flow. *Proc. Natl. Acad. Sci. USA*, 100(7):3841–3846 (electronic), 2003.

2. A. Arakawa. Computational design for long-term numerical integration of the equations of fluid motion: Two-dimensional incompressible flow. Part I. *J. Comput. Phys.*, 1:119–143, 1966.

3. J. Frank, G. Gottwald, and S. Reich. A Hamiltonian particle-mesh method for the rotating shallow-water equations. In *Meshfree Methods for Partial Differential Equations (Bonn, 2001)*, volume 26 of *Lect. Notes Comput. Sci. Eng.*, pages 131–142. Springer, Berlin, 2003.

4. J. Frank and S. Reich. Conservation properties of smoothed particle hydrodynamics applied to the shallow water equation. *BIT*, 43(1):41–55, 2003.

5. J. Frank and S. Reich. The Hamiltonian particle-mesh method for the spherical shallow water equations. *Atmos. Sci. Lett.*, 5:89–95, 2004.

6. E. Hairer, C. Lubich, and G. Wanner. *Geometric Numerical Integration*, volume 31 of *Springer Series in Computational Mathematics*. Springer-Verlag, Berlin, second edition, 2006. Structure-preserving algorithms for ordinary differential equations.

7. E. Hairer, S. P. Nørsett, and G. Wanner. *Solving Ordinary Differential Equations. I*, volume 8 of *Springer Series in Computational Mathematics*. Springer-Verlag, Berlin, second edition, 1993. Nonstiff problems.

8. R. H. Kraichnan. Statistical dynamics of two-dimensional flow. *J. Fluid Mech.*, 67:155–175, 1975.

9. B. Leimkuhler and S. Reich. *Simulating Hamiltonian Dynamics*, volume 14 of *Cambridge Monographs on Applied and Computational Mathematics*. Cambridge University Press, Cambridge, 2004.

10. E. N. Lorenz. Energy and numerical weather prediction. *Tellus*, 12, 1960.

11. A. J. Majda and X. Wang. *Non-linear Dynamics and Statistical Theories for Basic Geophysical Flows*. Cambridge University Press, Cambridge, 2006.

12. R. McLachlan. Symplectic integration of Hamiltonian wave equations. *Numer. Math.*, 66(4):465–492, 1994.

13. R. I. McLachlan. Explicit Lie-Poisson integration and the Euler equations. *Phys. Rev. Lett.*, 71(19):3043–3046, 1993.

14. P. J. Morrison. Hamiltonian description of the ideal fluid. *Rev. Modern Phys.*, 70(2):467–521, 1998.

15. Y. Nambu. Generalized Hamiltonian dynamics. *Phys. Rev. D (3)*, 7:2405–2412, 1973.

16. P. Névir and R. Blender. A Nambu representation of incompressible hydrodynamics using helicity and enstrophy. *J. Phys. A*, 26(22):L1189–L1193, 1993.

17. J. Pedlosky. *Geophysical Fluid Dynamics*. Springer, 2nd edition, 2005.

18. R. Salmon. *Lectures on Geophysical Fluid Dynamics*. Oxford University Press, New York, 1998.

19. R. Salmon. Poisson-bracket approach to the construction of energy- and potential-enstrophy-conserving algorithms for the shallow-water equations. *J. Atmospheric Sci.*, 61(16):2016–2036, 2004.

20. R. Salmon. A general method for conserving quantities related to potential vorticity in numerical models. *Nonlinearity*, 18(5):R1–R16, 2005.

21. R. Salmon, G. Holloway, and M. C. Hendershott. The equilibrium statistical mechanics of simple quasi-geostrophic models. *J. Fluid Mech.*, 75:691–703, 1976.

22. R. Salmon and L. D. Talley. Generalizations of Arakawa's Jacobian. *J. Comput. Phys.*, 83(2):247–259, 1989.

23. J. M. Sanz-Serna and M. P. Calvo. *Numerical Hamiltonian Problems*, volume 7 of *Applied Mathematics and Mathematical Computation*. Chapman & Hall, London, 1994.

24. A. M. Stuart and A. R. Humphries. *Dynamical Systems and Numerical Analysis*, volume 2 of *Cambridge Monographs on Applied and Computational Mathematics*. Cambridge University Press, Cambridge, 1996.

25. V. Zeitlin. Finite-mode analogs of 2D ideal hydrodynamics: coadjoint orbits and local canonical structure. *Phys. D*, 49(3):353–362, 1991.